

ArmGS: Composite Gaussian Appearance Refinement for Modeling Dynamic Urban Environments

Guile Wu, Dongfeng Bai, and Bingbing Liu
Huawei Noah's Ark Lab

{guile.wu, baidongfeng, liu.bingbing}@huawei.com



Figure 1. An illustration of our ArmGS for modeling urban scenes in autonomous driving. Our approach is capable of modeling fine-grained changes of background scenes and objects across frames and camera viewpoints.

Abstract

This work focuses on modeling dynamic urban environments for autonomous driving simulation. Contemporary data-driven methods using neural radiance fields have achieved photorealistic driving scene modeling, but they suffer from low rendering efficacy. Recently, some approaches have explored 3D Gaussian splatting for modeling dynamic urban scenes, enabling high-fidelity reconstruction and real-time rendering. However, these approaches often neglect to model fine-grained variations between frames and camera viewpoints, leading to suboptimal results. In this work, we propose a new approach named ArmGS that exploits composite driving Gaussian splatting with multi-granularity appearance refinement for autonomous driving scene modeling. The core idea of our approach is devising a multi-level appearance model-

ing scheme to optimize a set of transformation parameters for composite Gaussian refinement from multiple granularities, ranging from local Gaussian level to global image level and dynamic actor level. This not only models global scene appearance variations between frames and camera viewpoints, but also models local fine-grained changes of background and objects. Extensive experiments on multiple challenging autonomous driving datasets, namely, Waymo, KITTI, NOTR and VKITTI2, demonstrate the superiority of our approach over the state-of-the-art methods.

1. Introduction

Autonomous driving has made remarkable advancements in recent years, but how to effectively validate the safety and reliability of an autonomous driving system remains

an open question. In real-world driving scenes, there are many corner cases, such as collisions, which cannot be easily collected, but are critical to the safety of an autonomous driving system. Simulation is one of the most useful ways to alleviate this problem. It enables the reconstruction and generation of various challenging driving scenes for downstream closed-loop evaluation.

Traditionally, virtual-engine-based methods, such as CARLA [4], use classic graphics rendering systems for driving scene simulation, but the simulated scenes often have significant gaps from the real-world ones. On the other hand, data-driven simulation enables photorealistic driving scene modeling in a low-cost and efficient way [11, 27–30]. With the great success of Neural Radiance Fields (NeRFs) for neural rendering, some researchers have adapted NeRFs for scene modeling in autonomous driving [19, 27, 29, 30]. Although NeRF-based methods have shown great potential for reconstructing realistic driving scenes, they mostly suffer from long training time and fail to achieve real-time rendering. More recently, some researchers have resorted to 3D Gaussian Splatting (3DGS) [12] to learn explicit 3D scene representations for driving scene modeling [2, 11, 21, 28, 35]. Due to the efficiency of explicit representations and differentiable tile rasterizers, 3DGS-based methods have shown promising results for high-fidelity reconstruction and real-time rendering. However, existing approaches for driving scene modeling mostly neglect to model fine-grained driving scene variations between frames and camera viewpoints¹. In autonomous driving simulation, scene images are captured in the wild along the movement of the ego vehicle. This unavoidably brings significant appearance changes of scenes and objects across frames and camera viewpoints due to lighting and camera exposure. Thus, failing to model these variations can lead to missing fine-grained details and suboptimal simulation results.

In this work, we propose to exploit composite 3D Gaussian Splatting with Appearance RefineMent (ArmGS) from multiple granularities for dynamic urban environments modeling in autonomous driving. Our approach constructs a composite driving scene model based on 3DGS representations and employs a multi-level appearance modeling scheme to optimize a set of transformation parameters for composite Gaussian refinement. Specifically, we represent a driving scene with composite 3DGS and refine them at local Gaussian level, global image level and dynamic actor level, respectively. For local Gaussian level refinement, we extract latent Gaussian appearance representation to learn Gaussian-wise transformation parameters for Gaussian appearance refinement. This helps to learn local fine-grained appearance variations in the 3D Gaussian space. For global image level refinement, we extract latent image appear-

ance representation to learn global image-wise transformation parameters for image color refinement. This helps to learn global image-wise appearance changes across frames and camera viewpoints. Moreover, to model dynamic variations of moving road actors (such as vehicles), we employ a light-weight spatial-temporal deformation model to transform dynamic actor Gaussians across time. This multi-level appearance modeling scheme allows for refining the composite driving scene Gaussians at multiple granularities. Consequently, scene and road actors appearance variations are collectively modeled to reconstruct richer fine-grained cues of driving scenes. Our experiments on multiple challenging autonomous driving datasets, namely, Waymo [23], KITTI [8], NOTR [29] and VKITTI2 [1], for driving scene modeling and novel view synthesis show that our approach not only reconstructs global scene appearance variations between frames and camera viewpoints, but also models local fine-grained changes of background and dynamic objects. An illustration is shown in Fig. 1. In summary, our **contributions** are:

- Our method is the first method that proposes to explicitly embed multi-granularity appearances to model fine-grained changes for dynamic urban environments modeling. This fills a gap left by both existing NeRF and Gaussian splatting methods.
- Our method uses a set of transformation parameters for composite Gaussian refinement, which is simple and effective and will not break the differentiability of splatting.
- Our experiments on Waymo, KITTI, NOTR and VKITTI2 show the superiority of our method over the state-of-the-art methods.

2. Related Work

3D Gaussian Splatting. 3D Gaussian Splatting (3DGS) [12] is a recently proposed real-time rendering approach. Unlike NeRFs that employ a continuous radiance field to implicitly represent 3D scenes, 3DGS represents a 3D scene with a collection of explicit 3D Gaussian primitives and utilizes splatting-based rasterization [36] to project 3D Gaussians to 2D image space. Since the success of [12], researchers have made many efforts to improve 3DGS from different aspects [3, 5, 16, 31, 32], such as anti-aliasing [31], compression [5], surface reconstruction [16], etc. Among them, Dahmani *et al.* [3] propose to model image appearance changes with image embeddings for novel-view synthesis from unconstrained image collections. Our approach significantly differs from [3] in that we devise a novel multi-level appearance modeling scheme to optimize a set of transformation parameters for composite Gaussian refinement, rather than modeling transient objects and landmarks from unconstrained images. In addition, Wu *et al.* [26] propose to explore deformation fields with HexPlane representations for real-time dynamic 4D scene

¹Throughout this work, camera viewpoints refer to different locations of the same camera or different cameras

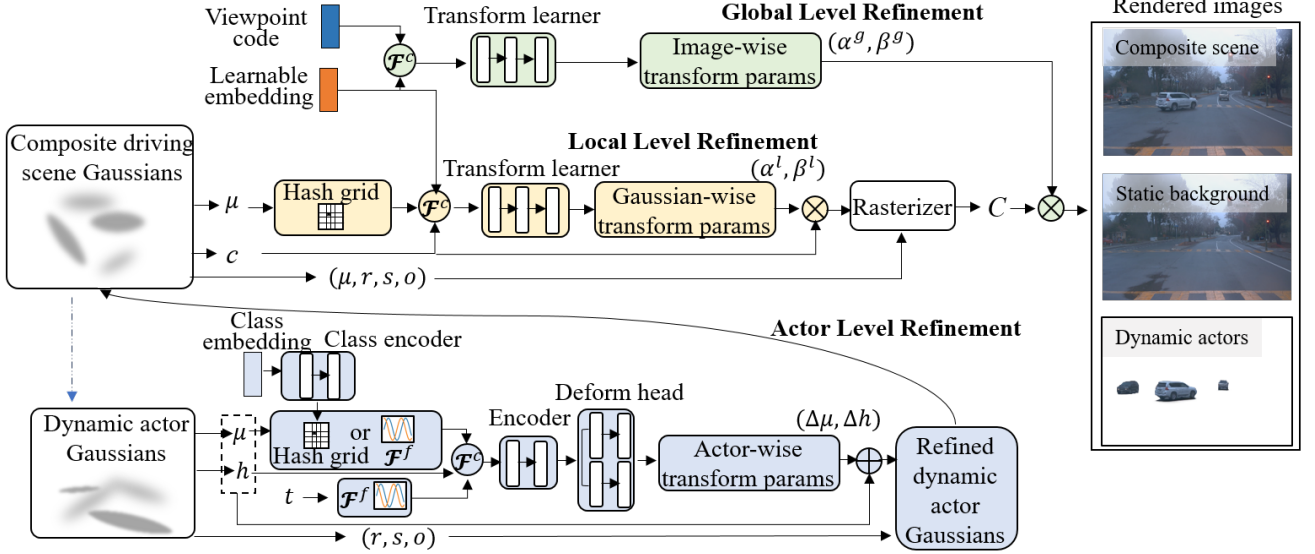


Figure 2. An overview of our ArmGS approach. Our approach refines composite driving scene Gaussians with appearance modeling at multiple granularities, ranging from local Gaussians level to global images level and dynamic actors level. The modules for local level refinement, global level refinement and actor level refinement are indicated in yellow, green and blue, respectively.

rendering, which is subsequently modified by [11] for dynamic urban scene reconstruction. Although we also employ deformation fields for dynamic actor level refinement, our method is different in that we construct a light-weight network structure and encode position, timestamp and spherical harmonics to learn actor variations, rather than constructing HexPlane representation [11, 26].

Autonomous Driving Scene Modeling. Autonomous driving simulation [4, 14, 15, 28–30] is critical for real-world closed-loop evaluation. For dynamic driving scene modeling, there are primarily two types of methods, namely, virtual-engine-based methods [1, 4] and data-driven methods [11, 28–30]. While virtual-engine-based methods typically lack scalability and suffer from significant domain gaps, data-driven methods are becoming prevailing in recent years due to their photo-realism, scalability and efficiency. For data-driven simulation, NeRF-based methods [7, 9, 19, 29] have shown compelling performance, but require point dense sampling along each ray to model the interaction between light and scene elements. This leads to expensive computational costs and low rendering speed. On the other hand, 3DGS-based methods [6, 11, 21, 28, 35] make full use of the advantages of 3DGS and achieve real-time rendering for modeling driving scenes. Yan *et al.* [28] proposes to model dynamic urban scenes with road asset pose optimization and 4D spherical harmonics appearance model, but neglects to model fine-grained driving scene variations between frames and camera viewpoints. Huang *et al.* [11] extends dynamic 4DGS [26] for driving scene reconstruction in a self-supervised manner, but the

rendering results are suboptimal with some artifacts and do not explicitly model fine-grained changes of driving scenes. Our work also builds on 3DGS, but different from existing works, our approach refines composite driving scene Gaussians with appearance modeling at multiple granularities, ranging from local Gaussians to global images and dynamic actors. Our approach is capable of modeling global scene appearance variations as well as local fine-grained changes of background and dynamic objects in autonomous driving scenes.

3. Methodology

3.1. Preliminaries

3D Gaussian Splatting. Formally, 3DGS [12] consists of a collection of learnable parameters, where each Gaussian is defined by the position (mean) parameter $\mu \in \mathbb{R}^3$, the covariance matrix Σ (which is determined by the rotation parameter $r \in \mathbb{R}^4$ and the scaling parameter $s \in \mathbb{R}^3$), the opacity parameter $o \in \mathbb{R}^1$ and the spherical harmonics parameter $h \in \mathbb{R}^d$ (d is determined by the degrees of spherical harmonics). These parameters collectively represent Gaussians in a 3D space as:

$$G(x) = e^{-\frac{1}{2}(x-\mu)^T \Sigma^{-1}(x-\mu)}, \quad (1)$$

where point x is centered at μ . To render images from different camera viewpoints, 3D Gaussians are projected onto the corresponding image plane and the color C of each pixel

is calculated with N -ordered 2D splats using α -blending as:

$$C = \sum_{i \in N} c_i \alpha_i \prod_{j=1}^{i-1} (1 - \alpha_j), \quad (2)$$

where c_i is the color derived from h and α_i is determined by o and the contribution of the Gaussian.

Composite Driving Scene Gaussians. Inspired by [19, 28, 34], we represent a driving scene with composite 3DGS models, including a background Gaussian model, dynamic actor Gaussian models and a sky Gaussian model. In the background Gaussian model, we use a set of 3D Gaussians to model the background scene in the world coordinate space. For each dynamic actor (such as moving vehicle) in a driving scene, we represent it with a separate Gaussian model in the object-centric coordinate space. These dynamic actor Gaussians are transformed to world coordinates with pose transformation matrices to form the composite scene Gaussians. For distant sky region, we construct the sky Gaussian model with explicit cubemap representations [28] and model sky color from view direction. These models collectively form the composite Gaussians to be rendered via a differentiable tile-based rasterizer.

Although composite scene Gaussians can reconstruct 3D driving scenes in an efficient way, existing methods [21, 28, 34] lack the ability to effectively model driving scene appearance variations between frames and camera viewpoints, leading to missing fine-grained details and suboptimal simulation results. To resolve this problem, we present composite 3DGS appearance refinement via a multi-level appearance modeling scheme.

3.2. Composite Driving Gaussian with Multi-Level Appearance Refinement

An overview of our ArmGS approach is depicted in Fig. 2. Our approach realizes driving scene appearance refinement from three levels, namely, local composite Gaussian level, global image level and dynamic actor level.

Local Composite Gaussian Level Refinement. With composite driving Gaussians, we propose to model fine-grained scene variations by learning a set of transformation parameters to refine composite Gaussians. First, to model changes across scene frames, we construct a low-dimensional learnable embedding ϵ for each frame. Then, we employ a multiresolution Hash grid \mathcal{H} [18] to extract richer Gaussian position code and merge the low-dimensional embedding, the position code and the Gaussian color as the *latent Gaussian appearance representation* f^l of each Gaussian. This is formulated as:

$$f^l = \mathcal{F}^c(\mathcal{H}(\mu), \epsilon, c), \quad (3)$$

where the merge function \mathcal{F}^c is concatenation in this work. Then, we employ a local Gaussian appearance affine transformation learner \mathcal{D}^l (a light-weight MLP) with f^l as the input to learn local Gaussian-wise transformation parameters ($\alpha^l \in \mathbb{R}^3, \beta^l \in \mathbb{R}^3$) for Gaussian appearance refinement, which is defined as:

$$c' = \alpha^l c + \beta^l, \quad \text{where } (\alpha^l, \beta^l) = \mathcal{D}^l(f^l). \quad (4)$$

c' is then used in Eq.(2) for color computation. In this way, the contribution of each Gaussian to the rendered image is modulated across frames, so fine-grained scene variations are effectively encoded into local Gaussian-wise appearance variations across frames. During rendering, to obtain a low-dimensional embedding ϵ for a novel view, we consider that the appearance variation of a novel view should be consistent with its adjacent frame. Thus, for each novel view, we calculate the index of its nearest neighbor training frames based on camera index and timestamp to get its corresponding ϵ , and then perform Eqs.(3) and (4) for the transformation.

Global Image Level Refinement. Although the local Gaussian-wise appearance refinement encourages each Gaussian to learn local fine-grained variations, it does not encourage global consistent variations across camera viewpoints. For example, image-wise appearance variation can be consistently changed due to direct sunlight or camera exposure, which requires the holistic scene appearance refinement. Thus, to compensate for the global image-wise variation, we further refine driving scene appearance at the global image level. Specifically, we encode camera location and viewing direction as a camera viewpoint code ϕ and merge it with the embedding ϵ as the *latent image appearance representation* f^g , which is defined as:

$$f^g = \mathcal{F}^c(\epsilon, \phi). \quad (5)$$

We then employ an image appearance affine transformation learner \mathcal{D}^g with f^g as the input to learn global image-wise transformation parameters ($\alpha^g \in \mathbb{R}^{3 \times 3}, \beta^g \in \mathbb{R}^{1 \times 3}$) for image color transformation, which is formulated as:

$$C' = \alpha^g C + \beta^g, \quad \text{where } (\alpha^g, \beta^g) = \mathcal{D}^g(f^g). \quad (6)$$

With the collaboration of local Gaussian-wise appearance modeling and global image-wise appearance modeling, the composite driving scene Gaussians are modulated at different granularities.

Dynamic Actor Level Refinement. In dynamic driving scene modeling, dynamic road actors usually have more complex motion and appearance variations than background and static objects. For example, a moving vehicle needs to be placed at different locations along its trajectory, while

its appearance is affected not only by the scene but also by its actions, such as using brake signals. To deal with this problem, we also refine composite driving Gaussians at the dynamic actor level. Specifically, we employ a low-dimensional learnable embedding for each class of dynamic actors and construct a light-weight class encoder to learn the weights of the dynamic actor Hash grid, inspired by [10, 30]. This helps to encode class information into Hash grid for position encoding. Alternatively, to reduce training parameters, we observe that the simple yet effective sinusoidal encoding [17] also works well. Then, to model the complex appearance variations specific to each dynamic actor, we construct a light-weight spatial-temporal encoder and a light-weight deformation head to transform position and spherical harmonics attributes of dynamic actor Gaussians across time. Instead of using the HexPlane [26] to learn the spatial-temporal structure, we encode position μ with the encoding function \mathcal{F}^a (class-wise Hash grid or sinusoidal encoding), timestamp t with a sinusoidal function \mathcal{F}^f and merge them with the spherical harmonics h to learn the *spatial-temporal actor representation* f^a of the dynamic actor. This is defined as:

$$f^a = \mathcal{D}^a(\mathcal{F}^c(\mathcal{F}^a(\mu), \mathcal{F}^f(t), h)), \quad (7)$$

where \mathcal{D}^a is a shared spatial-temporal representation encoder. Then, we use a deformation head (a multi-head MLP) \mathcal{D}^h with f^a as the input to learn deformation for Gaussian position and color refinement, as:

$$\{\mu', h'\} = \{\mu + \Delta\mu, h + \Delta h\}, \text{ where } \{\Delta\mu, \Delta h\} = \mathcal{D}^h(f^a). \quad (8)$$

Note that, although Gaussian deformation is inspired by [26], our design differs from existing works [6, 11, 26] in that we construct light-weight encoders and deformation heads and encodes position, timestamp and spherical harmonics to learn actor variations, rather than constructing HexPlane representation [11, 26] or using neural fields for color computation [6]. Moreover, the collaboration of the local level refinement, the global level refinement and the dynamic actor level refinement brings superior performance for dynamic urban environments modeling in autonomous driving.

3.3. Composite Driving Gaussian Optimization

Training Objective. We optimize our approach in an end-to-end differentiable rendering manner. The training objective loss is defined as:

$$\mathcal{L} = (1 - \lambda_1)\mathcal{L}_{rgb} + \lambda_1\mathcal{L}_{ssim} + \lambda_2\mathcal{L}_d + \lambda_3\mathcal{L}_s + \lambda_4\mathcal{L}_f, \quad (9)$$

where λ_i is the weight coefficient, \mathcal{L}_{rgb} and \mathcal{L}_{ssim} are the image reconstruction loss between rendering images and ground-truth images following [12], \mathcal{L}_d is a depth loss calculated by a L1 loss between rendering depth maps and LiDAR depth, \mathcal{L}_s is a sky mask loss computed by a binary

cross-entropy loss between rendering sky masks and pre-extracted sky masks [20], and \mathcal{L}_f is a foreground decomposition loss [28] calculated by an entropy loss on the accumulated alpha values of dynamic actors.

Actor Pose Optimization. For pose transformation parameters (the rotation quaternion R_t and the translation T_t) of each actor, we set them as learnable parameters and initialize them with the provided tracked boxes. The position and rotation of each Gaussian of each actor in the world space are defined as $\mu = R_t\mu^a + T_t$ and $r = R_tr^a$, where μ^a and r^a are dynamic actor poses in the object-centric coordinate space. These transformation parameters are directly optimized with scene reconstruction through gradient back-propagation. When rendering novel views, we interpolate actor poses based on timestamps and the optimized poses.

4. Experiment

4.1. Datasets and Evaluation Protocol

Datasets. We conduct experiments on four challenging autonomous driving datasets, including the Waymo [23, 28], KITTI [8], NOTR [29] and Virtual KITTI 2 (VKITTI2) [1]. On Waymo, following [28], we select eight challenging sequences with dynamic actors and complex background and use the tracked boxes provided by [28] for experiments. We select every fourth frame as the testing novel view and use the remaining frames as the training views. We set the image resolution to 1066×1600 and evaluate both the novel view synthesis setting with the testing views and the image reconstruction setting with the training views. On KITTI, following [7, 24], we select three sequences and use the official tracklets for evaluation in the novel view synthesis setting. We select every second frame as the testing novel view while the others are used for training. The image resolution is set to 375×1242. On NOTR, following [29], we employ two splits, namely, the static-32 and dynamic-32 splits, which consist of 64 multi-camera driving scene sequences with various challenges, *e.g.*, cross-camera background variations, various dynamic actors, *etc.* The image resolution is set to 640×960. On VKITTI2, following [34], we select two sequences for experiments and use the 50% dropout rate evaluation protocol. The image resolution is set to 375×1242.

Evaluation Metrics. Following [11, 28, 29, 34], we use PSNR, SSIM [25] and LPIPS [33] as the evaluation metrics.

Compared Methods. We compare our ArmGS approach with several state-of-the-art methods which can be categorized into two types: (1) 3DGS-based methods, including StreetGaussians [28], S³Gaussian [11], 3DGS [12] and HUGS [34]; (2) NeRF-based methods, including EmerNerf [29], ML-NSG [7], SUDS [24], NSG [19], Street-

Method	Waymo Novel View			Waymo Reconstruction			KITTI		
	PSNR \uparrow	SSIM \uparrow	LPIPS \downarrow	PSNR \uparrow	SSIM \uparrow	LPIPS \downarrow	PSNR \uparrow	SSIM \uparrow	LPIPS \downarrow
NSG [19]	28.3	0.862	0.346	-	-	-	21.3	0.659	0.266
SUDS [24]	-	-	-	-	-	-	23.1	0.821	0.135
3DGS [12]	29.6	0.918	0.117	32.5	0.938	0.089	19.2	0.739	0.174
S ³ Gaussian [11]	32.8	0.931	0.097	35.6	0.946	0.088	-	-	-
EmerNeRF [29]	30.9	0.905	0.133	34.5	0.913	0.123	-	-	-
ML-NSG [7]	-	-	-	-	-	-	27.5	0.898	0.055
StreetGaussians [28]	34.6	0.938	0.079	36.3	0.948	0.074	27.8	0.889	0.069
ArmGS (Ours)	35.7	0.944	0.074	38.1	0.957	0.064	30.3	0.931	0.036

Table 1. Quantitative comparison with the state-of-the-art methods on the Waymo and KITTI datasets.

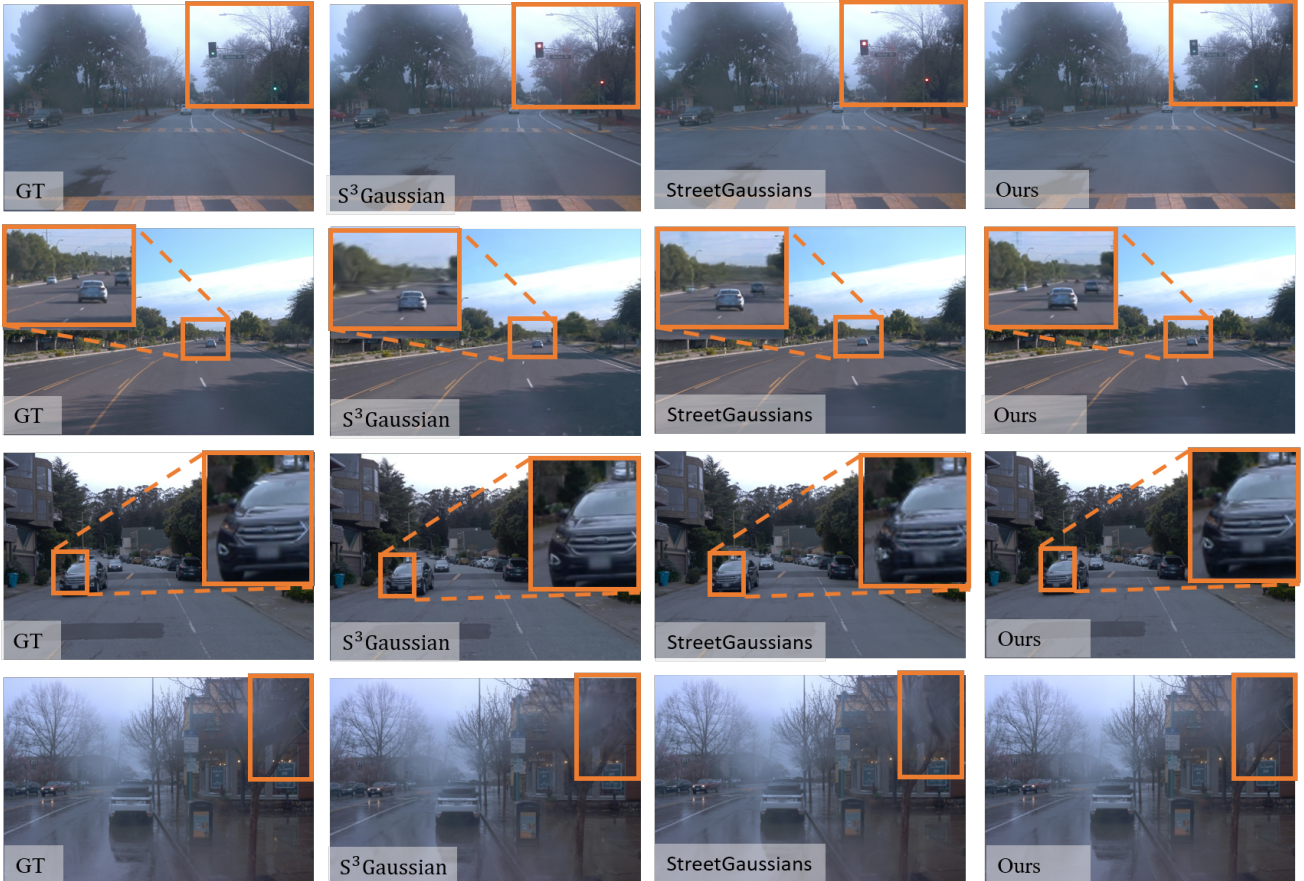


Figure 3. Qualitative comparison with the state-of-the-arts on the Waymo dataset. From the first column to the fourth column, we show results for GT, S³Gaussian, StreetGaussians and Ours, respectively. We highlight some fine-grained details, *e.g.*, traffic lights, vehicles and trees.

Surf [9] and MARS [27]. Please refer to the supplementary material for the implementation details of our approach.

4.2. Evaluation on Waymo

We present the quantitative results on Waymo in Tab. 1. We can see that our approach achieves significantly better performance compared with the state-of-the-arts in both

the novel view synthesis and the image reconstruction settings. Specifically, for image reconstruction, our approach achieves the best PSNR of 38.1 dB, SSIM of 0.957 and LPIPS of 0.064, outperforming the state-of-the-art competitors, such as StreetGaussians and EmerNeRF. For novel view synthesis, our approach still achieves the best results compared with the state-of-the-art methods. For instance,

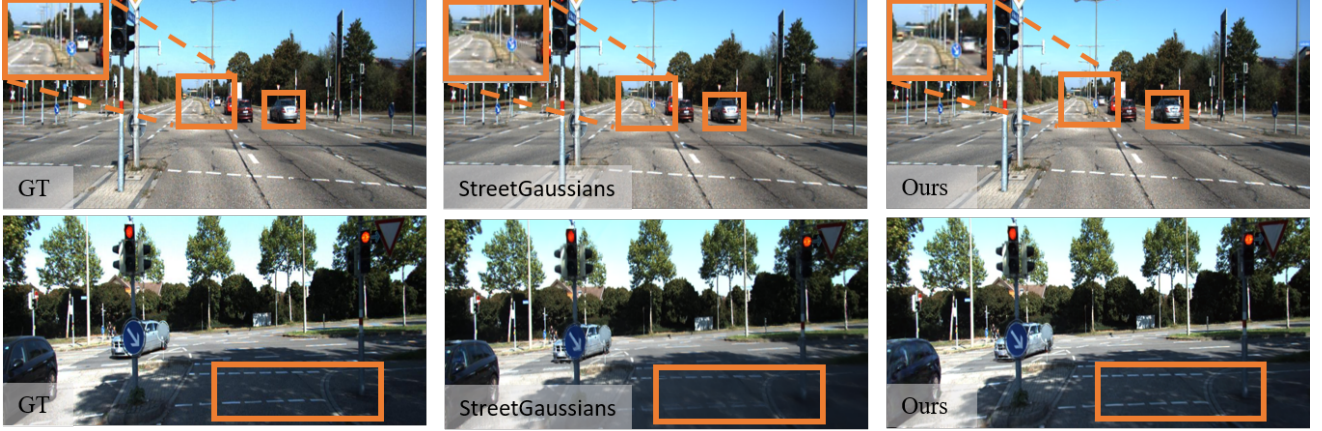


Figure 4. Qualitative comparison with the state-of-the-art methods on the KITTI dataset. From the first column to the 3th column, we show results for GT, StreetGaussians and Ours, respectively. We highlight some fine-grained details, *e.g.*, vehicles and lane lines.



Figure 5. Qualitative comparison on the NOTR dataset. We highlight some fine-grained details, *e.g.*, vehicles and pedestrians.

our approach achieves PSNR of 35.7 dB, which significantly surpass the second-best StreetGaussians by 1.1 dB. Furthermore, in Fig. 3, we present some qualitative results of scene modeling under foggy, sunny, cloudy and rainy conditions on Waymo. It can be seen that our approach renders more fine-grained details of the background scenes and dynamic actors. For example, as shown in the first row, most methods fail to render the appearance change of traffic lights, while our approach render this fine-grained variation; and as shown in the second row, our approach is able to model appearance of the distant vehicles, while other methods render results with artifacts. Moreover, our experimental results show that the rendering speeds of the compared NeRF-based methods, *e.g.*, EmerNeRF, are usually less than 1 FPS; in comparison, the 3DGS-based methods (including our approach) are able to achieve real-time rendering ($>30\text{FPS}$).

4.3. Evaluation on KITTI

We report the quantitative and qualitative results on the KITTI dataset in Tab. 1 and Fig. 4, respectively. Overall, our approach achieves significantly better performance compared with the state-of-the-art methods. Specifically, from Tab. 1, we can see that our approach achieves the best PSNR of 30.3 dB, SSIM of 0.931 and LPIPS of 0.036, significantly outperforming the state-of-the-art methods. Furthermore, from Fig. 4, we can see that compared with StreetGaussians, our approach is able to render better image quality with more fine-grained details, such as vehicles highlighted in the first row and the lane line highlighted in the second row.

4.4. Evaluation on NOTR

To further probe the upper bound reconstruction capability of our approach, we follow [29] to conduct the scene reconstruction experiment on the NOTR dataset [29]. We

Method	Static-32	Dynamic-32
StreetSurf [9]	26.2	-
EmerNeRF [29]	29.1	28.9
StreetGaussians [28]	29.6	29.7
ArmGS (Ours)	30.5	30.5

Table 2. Results on the NOTR dataset. PSNRs are reported.

Method	PSNR \uparrow	SSIM \uparrow	LPIPS \downarrow
NSG [19]	21.0	0.704	0.316
MARS [27]	22.2	0.869	0.131
3DGS [12]	20.6	0.892	0.103
HUGS [34]	26.4	0.916	0.035
ArmGS (Ours)	31.1	0.957	0.016

Table 3. Results on the VKITTI2 dataset.

report the quantitative and qualitative results in Tab. 2 and Fig. 5, respectively. As shown in Tab. 2, compared with the state-of-the-art StreetSurf [9], EmerNeRF [29] and StreetGaussians [28], our approach achieves better performance on both the static-32 and dynamic-32 splits. From Fig. 5, we can see that our approach is able to model fine-grained details of driving scenes across cameras; in comparison, StreetGaussians renders driving scenes with more artifacts, such as blurred vehicles. These results indicate that our approach is able to faithfully model complex driving scenes and render high-quality results.

4.5. Evaluation on VKITTI2

Our approach is not limited to modeling real-world driving scenes, but can also be used to model synthetic driving scenes. To show the performance of our approach for synthetic driving scenes modeling, we follow [34] conducting experiments on the VKITTI2 dataset [1]. We report the results in Tab. 3. Although synthetic scenes usually have fewer appearance changes of scenes and objects across frames, our approach still achieves better results compared with the state-of-the-art HUGS, demonstrating the superiority of our approach. These results indicate that our approach is also applicable to synthetic driving scene modeling.

4.6. Ablation Study

Dynamic Actor Modeling Effectiveness Analysis. To evaluate the effectiveness of our dynamic actor level refinement, we follow [28] projecting the 3D bounding box onto the 2D image plane to obtain the mask regions of moving objects and compute PSNR within the mask regions. This mitigates the effect of background on dynamic actors when evaluating dynamic actors. As shown in Tab. 4, our approach achieves better results for the rendered dynamic actor regions compared with StreetGaussians and EmerN-

Method	Novel	Recon.
Ours	30.9	35.8
Ours w/ class-wise actor encoding	30.9	35.7
Ours w/o dynamic actor refinement	30.7	35.4
Ours w/ 4DGS HexPlane [26]	30.6	35.7
EmerNeRF [29]	21.7	26.8
StreetGaussians [28]	30.2	34.8

Table 4. Effectiveness analysis of dynamic actor modeling on the Waymo dataset. PSNRs of the moving object regions are reported.

Method	Novel	Recon.
Ours	35.7	38.1
Ours w/o local level refinement	35.0	36.8
Ours w/o global level refinement	35.4	37.7
Ours w/ HUGS appearance [34]	34.8	36.5

Table 5. Effectiveness analysis of local and global appearance refinement on the Waymo Dataset. Results are in terms of PSNR.

eRF. When using class-wise actor encoding, our approach achieves similar performance, but when dynamic actor level refinement is not used, the PSNRs of our approach are reduced by 0.4 dB and 0.2 dB in the reconstruction and novel view synthesis setting, respectively. When replacing our dynamic actor level refinement design with the 4DGS HexPlane [26], the results are still worse than our design.

Local and Global Appearance Refinement Effectiveness Analysis. In Tab. 5, we evaluate the effectiveness of the local composite Gaussian level refinement and the global image level refinement. It can be seen that our approach with both local and global appearance refinement performs the best, while without using local level refinement or global level refinement, the performance of our approach degrades. Besides, using HUGS appearance modeling in lieu of our design results in worse performance. These results verify the effectiveness of our design.

5. Conclusion

This work presents a composite Gaussian appearance refinement approach (ArmGS) to urban environments modeling for autonomous driving simulation. The key idea is to learn a set of transformation parameters to refine 3D Gaussians from multi-level granularities, ranging from local Gaussian level to global image level and dynamic actor level. Our thorough experiments on four autonomous driving datasets demonstrate that our approach is capable of rendering more fine-grained details of driving scenes across frames and camera viewpoints, achieving superior performance compared with the state-of-the-art methods.

References

- [1] Yohann Cabon, Naila Murray, and Martin Humenberger. Virtual kitti 2. *arXiv preprint arXiv:2001.10773*, 2020. 2, 3, 5, 8
- [2] Yurui Chen, Chun Gu, Junzhe Jiang, Xiatian Zhu, and Li Zhang. Periodic vibration gaussian: Dynamic urban scene reconstruction and real-time rendering. *arXiv preprint arXiv:2311.18561*, 2023. 2
- [3] Hiba Dahmani, Moussab Bennehar, Nathan Piasco, Luis Roldao, and Dzmitry Tsishkou. Swag: Splatting in the wild images with appearance-conditioned gaussians. In *ECCV*, 2024. 2
- [4] Alexey Dosovitskiy, German Ros, Felipe Codevilla, Antonio Lopez, and Vladlen Koltun. Carla: An open urban driving simulator. In *Conference on robot learning*, pages 1–16. PMLR, 2017. 2, 3
- [5] Zhiwen Fan, Kevin Wang, Kairun Wen, Zehao Zhu, DeJia Xu, and Zhangyang Wang. Lightgaussian: Unbounded 3d gaussian compression with 15x reduction and 200+ fps. In *Advances in Neural Information Processing Systems*, 2024. 2
- [6] Tobias Fischer, Jonas Kulhanek, Samuel Rota Bulò, Lorenzo Porzi, Marc Pollefeys, and Peter Kotschieder. Dynamic 3d gaussian fields for urban areas. In *Advances in Neural Information Processing Systems*, 2024. 3, 5
- [7] Tobias Fischer, Lorenzo Porzi, Samuel Rota Bulò, Marc Pollefeys, and Peter Kotschieder. Multi-level neural scene graphs for dynamic urban environments. In *Proceedings of the IEEE/CVF Conference on Computer Vision and Pattern Recognition*, pages 21125–21135, 2024. 3, 5, 6
- [8] Andreas Geiger, Philip Lenz, and Raquel Urtasun. Are we ready for autonomous driving? the kitti vision benchmark suite. In *2012 IEEE conference on computer vision and pattern recognition*, pages 3354–3361. IEEE, 2012. 2, 5
- [9] Jianfei Guo, Nianchen Deng, Xinyang Li, Yeqi Bai, Botian Shi, Chiyu Wang, Chenjing Ding, Dongliang Wang, and Yikang Li. Streetsurf: Extending multi-view implicit surface reconstruction to street views. *arXiv preprint arXiv:2306.04988*, 2023. 3, 6, 8
- [10] David Ha, Andrew Dai, and Quoc V Le. Hypernetworks. *arXiv preprint arXiv:1609.09106*, 2016. 5
- [11] Nan Huang, Xiaobao Wei, Wenzhao Zheng, Pengju An, Ming Lu, Wei Zhan, Masayoshi Tomizuka, Kurt Keutzer, and Shanghang Zhang. S³gaussian: Self-supervised street gaussians for autonomous driving. *arXiv preprint arXiv:2405.20323*, 2024. 2, 3, 5, 6
- [12] Bernhard Kerbl, Georgios Kopanas, Thomas Leimkühler, and George Drettakis. 3d gaussian splatting for real-time radiance field rendering. *ACM Transactions on Graphics*, 42(4):1–14, 2023. 2, 3, 5, 6, 8, 1
- [13] Diederik P Kingma. Adam: A method for stochastic optimization. *arXiv preprint arXiv:1412.6980*, 2014. 1
- [14] Yibo Liu, Kelly Zhu, Guile Wu, Yuan Ren, Bingbing Liu, Yang Liu, and Jinjun Shan. Mv-deepsdf: Implicit modeling with multi-sweep point clouds for 3d vehicle reconstruction in autonomous driving. In *Proceedings of the IEEE/CVF International Conference on Computer Vision*, pages 8306–8316, 2023. 3
- [15] Yibo Liu, Zheyuan Yang, Guile Wu, Yuan Ren, Kejian Lin, Bingbing Liu, Yang Liu, and Jinjun Shan. Vqa-diff: Exploiting vqa and diffusion for zero-shot image-to-3d vehicle asset generation in autonomous driving. In *European Conference on Computer Vision*, pages 323–340. Springer, 2024. 3
- [16] Xiaoyang Lyu, Yang-Tian Sun, Yi-Hua Huang, Xiuzhe Wu, Ziyi Yang, Yilun Chen, Jiangmiao Pang, and Xiaojuan Qi. 3dgsr: Implicit surface reconstruction with 3d gaussian splatting. *ACM Transactions on Graphics (TOG)*, 43(6):1–12, 2024. 2
- [17] Ben Mildenhall, Pratul P Srinivasan, Matthew Tancik, Jonathan T Barron, Ravi Ramamoorthi, and Ren Ng. Nerf: Representing scenes as neural radiance fields for view synthesis. *Communications of the ACM*, 65(1):99–106, 2021. 5
- [18] Thomas Müller, Alex Evans, Christoph Schied, and Alexander Keller. Instant neural graphics primitives with a multi-resolution hash encoding. *ACM transactions on graphics (TOG)*, 41(4):1–15, 2022. 4
- [19] Julian Ost, Fahim Mannan, Nils Thuerey, Julian Knodt, and Felix Heide. Neural scene graphs for dynamic scenes. In *Proceedings of the IEEE/CVF Conference on Computer Vision and Pattern Recognition*, pages 2856–2865, 2021. 2, 3, 4, 5, 6, 8
- [20] Tianhe Ren, Shilong Liu, Ailing Zeng, Jing Lin, Kunchang Li, He Cao, Jiayu Chen, Xinyu Huang, Yukang Chen, Feng Yan, et al. Grounded sam: Assembling open-world models for diverse visual tasks. *arXiv preprint arXiv:2401.14159*, 2024. 5
- [21] Yuan Ren, Guile Wu, Runhao Li, Zheyuan Yang, Yibo Liu, Xingxin Chen, Tongtong Cao, and Bingbing Liu. Unigaussian: Driving scene reconstruction from multiple camera models via unified gaussian representations. *arXiv preprint arXiv:2411.15355*, 2024. 2, 3, 4
- [22] Johannes L Schonberger and Jan-Michael Frahm. Structure-from-motion revisited. In *Proceedings of the IEEE conference on computer vision and pattern recognition*, pages 4104–4113, 2016. 1
- [23] Pei Sun, Henrik Kretzschmar, Xerxes Dotiwalla, Aurelien Chouard, Vijaysai Patnaik, Paul Tsui, James Guo, Yin Zhou, Yuning Chai, Benjamin Caine, et al. Scalability in perception for autonomous driving: Waymo open dataset. In *Proceedings of the IEEE/CVF conference on computer vision and pattern recognition*, pages 2446–2454, 2020. 2, 5
- [24] Haithem Turki, Jason Y Zhang, Francesco Ferroni, and Deva Ramanan. Suds: Scalable urban dynamic scenes. In *Proceedings of the IEEE/CVF Conference on Computer Vision and Pattern Recognition*, pages 12375–12385, 2023. 5, 6
- [25] Zhou Wang, Alan C Bovik, Hamid R Sheikh, and Eero P Simoncelli. Image quality assessment: from error visibility to structural similarity. *IEEE transactions on image processing*, 13(4):600–612, 2004. 5
- [26] GuanJun Wu, Taoran Yi, Jiemin Fang, Lingxi Xie, Xiaopeng Zhang, Wei Wei, Wenyu Liu, Qi Tian, and Xinggang Wang. 4d gaussian splatting for real-time dynamic scene rendering.

- In *Proceedings of the IEEE/CVF Conference on Computer Vision and Pattern Recognition*, pages 20310–20320, 2024. [2](#), [3](#), [5](#), [8](#)
- [27] Zirui Wu, Tianyu Liu, Liyi Luo, Zhide Zhong, Jianteng Chen, Hongmin Xiao, Chao Hou, Haozhe Lou, Yuantao Chen, Runyi Yang, et al. Mars: An instance-aware, modular and realistic simulator for autonomous driving. In *CAAI International Conference on Artificial Intelligence*, pages 3–15. Springer, 2023. [2](#), [6](#), [8](#)
 - [28] Yunzhi Yan, Haotong Lin, Chenxu Zhou, Weijie Wang, Haiyang Sun, Kun Zhan, Xianpeng Lang, Xiaowei Zhou, and Sida Peng. Street gaussians: Modeling dynamic urban scenes with gaussian splatting. In *ECCV*, 2024. [2](#), [3](#), [4](#), [5](#), [6](#), [8](#), [1](#)
 - [29] Jiawei Yang, Boris Ivanovic, Or Litany, Xinshuo Weng, Seung Wook Kim, Boyi Li, Tong Che, Danfei Xu, Sanja Fidler, Marco Pavone, et al. Emernerf: Emergent spatial-temporal scene decomposition via self-supervision. In *International Conference on Learning Representations*, 2024. [2](#), [3](#), [5](#), [6](#), [7](#), [8](#)
 - [30] Ze Yang, Yun Chen, Jingkan Wang, Sivabalan Manivasagam, Wei-Chiu Ma, Anqi Joyce Yang, and Raquel Urtasun. Unisim: A neural closed-loop sensor simulator. In *Proceedings of the IEEE/CVF Conference on Computer Vision and Pattern Recognition*, pages 1389–1399, 2023. [2](#), [3](#), [5](#)
 - [31] Zehao Yu, Anpei Chen, Binbin Huang, Torsten Sattler, and Andreas Geiger. Mip-splatting: Alias-free 3d gaussian splatting. In *Proceedings of the IEEE/CVF Conference on Computer Vision and Pattern Recognition*, pages 19447–19456, 2024. [2](#)
 - [32] Dongbin Zhang, Chuming Wang, Weitao Wang, Peihao Li, Minghan Qin, and Haoqian Wang. Gaussian in the wild: 3d gaussian splatting for unconstrained image collections. *arXiv preprint arXiv:2403.15704*, 2024. [2](#)
 - [33] Richard Zhang, Phillip Isola, Alexei A Efros, Eli Shechtman, and Oliver Wang. The unreasonable effectiveness of deep features as a perceptual metric. In *Proceedings of the IEEE conference on computer vision and pattern recognition*, pages 586–595, 2018. [5](#)
 - [34] Hongyu Zhou, Jiahao Shao, Lu Xu, Dongfeng Bai, Weichao Qiu, Bingbing Liu, Yue Wang, Andreas Geiger, and Yiyi Liao. Hugs: Holistic urban 3d scene understanding via gaussian splatting. In *Proceedings of the IEEE/CVF Conference on Computer Vision and Pattern Recognition*, pages 21336–21345, 2024. [4](#), [5](#), [8](#)
 - [35] Xiaoyu Zhou, Zhiwei Lin, Xiaojun Shan, Yongtao Wang, Deqing Sun, and Ming-Hsuan Yang. Drivinggaussian: Composite gaussian splatting for surrounding dynamic autonomous driving scenes. In *Proceedings of the IEEE/CVF Conference on Computer Vision and Pattern Recognition*, pages 21634–21643, 2024. [2](#), [3](#)
 - [36] Matthias Zwicker, Hanspeter Pfister, Jeroen Van Baar, and Markus Gross. Ewa volume splatting. In *Proceedings Visualization, 2001. VIS'01.*, pages 29–538. IEEE, 2001. [2](#)

ArmGS: Composite Gaussian Appearance Refinement for Modeling Dynamic Urban Environments

Supplementary Material

In this supplementary material, we present implementation details of our approach in Sec. 6, show more experimental analysis and discussion in Sec. 7, and discuss the limitation and future work of our approach in Sec. 8.

6. Implementation Details

We implement our approach with Python and PyTorch. We initialize driving scene Gaussians with LiDAR point clouds and SfM points extracted by COLMAP [22], and train our model with 30000 iterations using the Adam [13] optimizer. We set the initial position learning rate to $1.6e^{-4}$ and decay to $1.6e^{-6}$, while the learning rates for rotation, scaling, opacity and spherical harmonics are set to $1e^{-3}$, $5e^{-3}$, $5e^{-2}$ and $2.5e^{-3}$, respectively. We construct the local affine transformation learner with three linear layers, the global affine transformation learner with four linear layers and the class encoder with two linear layers, where ReLU activations are used between layers. For the spatial-temporal encoder and the deformation head, we employ two linear layers with ReLU activations between layers. By default, we use \mathcal{F}^f for dynamic actor position encoding. For training objective loss, we empirically set $\lambda_1=0.2$, $\lambda_2=0.01$, $\lambda_3=0.05$ and $\lambda_4=0.1$. Following [12], Gaussian splitting and merging for adaptive density control are performed every 100 iterations from 500 iterations and until 15000 iterations.

7. Further Analysis and Discussion

Novel View Synthesis with Lane Shift Evaluation. We evaluate the performance of our approach for the extrapolated novel view synthesis by moving the ego-vehicle to left or right by 1, 2 and 3 meters. As shown in Tab. 6, our approach achieves lower FIDs than StreetGaussians under different lane shift distances. From Fig. 6, we can see that our approach produces fewer rendering artifacts for extrapolated novel views synthesis. These results indicate that our approach is capable of simulating extrapolated novel views with better quality.

Driving Scene Decomposition. In Fig. 7, we show the results of our approach for driving scene decomposition of static background and dynamic actors. It can be seen that our approach can well separate static background and dynamic actors. This indicates that although background and dynamic actors are jointly optimized with the multi-level appearance modeling scheme in our approach, this scheme

Method	FID↓@1m	FID↓@2m	FID↓@3m
ArmGS (Ours)	73.1	104.5	128.1
StreetGaussians [28]	81.8	113.3	140.2

Table 6. Lane shift evaluation on the Waymo dataset.



Figure 6. Novel view synthesis with lane shift evaluation on the Waymo dataset.



Figure 7. Driving scene decomposition results of our approach.

does not cause the background Gaussians and dynamic actor Gaussians to interfere with each other.

Driving Scene Editing. In Fig. 8, we show some examples of driving scene editing with our rendering results, including swapping positions of dynamic vehicles in a driving scene or synthesizing a corner case of vehicles driving in the wrong lane. From Fig. 8, we can see that these edited scenes are still photorealistic. These results show that our approach can potentially benefit other downstream autonomous driving simulation tasks, such as synthesizing challenging corner cases.

8. Limitation and Future Work

Despite the promising performance, our approach still has limitations. Specifically, our approach is limited to rendering images and lacks the ability to simulate LiDAR point clouds. How to simulate high-fidelity LiDAR point clouds

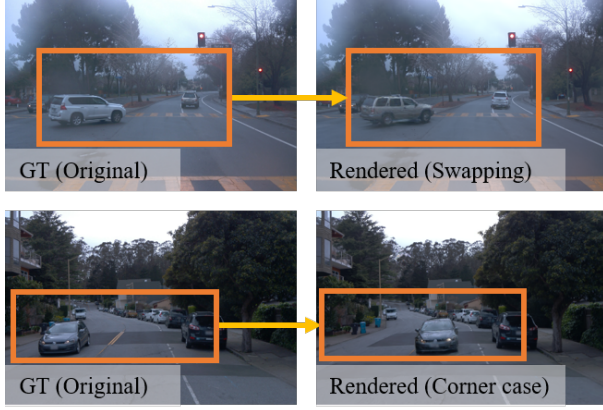


Figure 8. Examples of driving scene editing with our rendering results. The first row shows rendered results by swapping the vehicles and the second row shows synthesizing a corner case of vehicles driving in the wrong lane.

with 3DGS for autonomous driving scene modeling remains an open question. Besides, incorporating our approach into an autonomous driving simulator for closed-loop evaluation is an interesting direction. This can help to test the safety and reliability of autonomous vehicles. Our future work aims to solve these problems and build a comprehensive autonomous driving simulator.